Preparation of CO-tolerant anode electrocatalysts for polymer electrolyte membrane fuel cells

International Journal of Hydrogen Energy, Volume 42 (2017) 13741-13753.

Dorottya Gubán, András Tompos, István Bakos, Ádám Vass, Zoltán Pászti, Ervin Gy. Szabó, István E. Sajó, Irina Borbáth

http://dx.doi.org/10.1016/j.ijhydene.2017.03.080

Corresponding author: Irina Borbáth

Article history: Received 14 October 2016 / Received in revised form 10 March 2017 / Accepted 11 March 2017 / Available online 4 April 2017

Appendix A. Supplementary data

Supplementary data related to this article can be found at http://dx.doi.org/10.1016/j.ijhydene.2017.03.080

Preparation of CO-tolerant anode electrocatalysts for polymer electrolyte membrane fuel cells

D. Gubán[1], A. Tompos[1], I. Bakos[1], Á. Vass[1], Z. Pászti[1], E.Gy. Szabó[1], I.E. Sajó[2], I. Borbáth[1*]

[1]*Institute of Materials and Environmental Chemistry, Research Centre for Natural Sciences, Hungarian Academy of Sciences, H-1117 Budapest, Magyar tudósok körútja 2, Hungary,*
[2]*University of Pécs, Szentágothai Research Centre, Pécs, H-7624, Ifjúság str. 20. Hungary,*

Abstract:

The preparation and the thorough characterization of 40 wt% Pt electrocatalysts supported on $Ti_{(1-x)}M_xO_2$-C (M= W, Mo; x= 0.3-0.4) composite materials with enhanced stability and efficiency is presented.

W-containing composite supported catalyst with different structural characteristics were compared in order to explore the influence of the nature of the W species on the electrocatalytic performance. The assessment of the electrochemical properties of the novel catalysts revealed a correlation between the degree of W incorporation, the hydrogen spillover effect and the stability against initial leaching which influences the activity and CO tolerance of the catalysts.

A preparation route for $Ti_{0.7}Mo_{0.3}O_2$-C composite with high extent of Mo incorporation was developed. No significant difference was observed in the activity, stability and CO tolerance of the W- or Mo-containing composite supported Pt catalysts with almost complete incorporation of the oxophilic dopant. Better performance of the Pt/$Ti_{0.7}M_{0.3}O_2$-C (M= W, Mo) electrocatalysts in a single cell test device using hydrogen containing 100 ppm CO compared to the reference Pt/C and PtRu/C (Quintech) catalysts was also demonstrated.

Keywords: Anode electrocatalysts, $TiWO_x$, $TiMoO_x$, Conducting Ti-based mixed oxides, Composite materials, CO-tolerance

[*] Corresponding author, Tel.: +36 1 382 6916, email: borbath.irina@ttk.mta.hu, address: H-1519 Budapest, P.O.Box 286, Hungary (Irina Borbáth)

1. Introduction

Electrocatalysts, being responsible for facilitating oxidation of the fuel at the anode and reduction of oxygen at the cathode, are key components of fuel cells. In polymer electrolyte membrane (PEM) fuel cells activated carbon supported Pt catalysts with high metal loadings are commonly used both at the anode and the cathode. However, Pt/C catalysts suffer from severe drawbacks regarding stability (resistance to sintering or electrochemical corrosion) [1-5] and tolerance to CO poisoning, which is important as a small amount of CO is inevitably present in fuels obtained by reforming. These issues contribute to keeping the price of PEM fuel cells high and hindering their widespread application. It is therefore important to explore alternative materials that can provide improved stability.

Oxide supports are widely used in heterogeneous catalysis and have inherently higher stability than carbon in acidic and oxidizing environments [6,7]. Titanium dioxide is non-toxic, possesses high mechanical, chemical and redox stability [8,9]. Moreover, TiO_2 is also capable to stabilize metals in a highly dispersed state [10]. However, TiO_2 is an n-type semiconductor [11,12] and therefore for electrochemical applications the increase of electronic conductivity in TiO_2 is necessarily required. Doping of titania with n-type dopants such as transition metals (e.g., W, Nb and Ta) has been extensively used to enhance its electrical conductivity [13-17]. Most of the doped titania materials have electronic conductivities in the interval 0.1-1 S cm^{-1} (still substantially lower than carbon catalyst supports), but show high electrochemical stability and unique CO-tolerant electrocatalytic activity. In Ref. [18] sufficient conductivity of $Ti_{0.7}W_{0.3}O_2$ mixed oxide was ensured by mixing it with carbon powder. Materials composed of Pt nanoparticles, TiO_2 and carbon materials are identified as efficient electrocatalysts since they combine the high conductivity of carbon and corrosion resistance of the oxide with the synergistic effect between metal oxides and Pt [19].

Recently, the combination of highly stable TiO_2 with MoO_x, noted for its high electronic conductivity and relative stability in acid solutions, was used for the preparation of multifunctional $Ti_{0.7}Mo_{0.3}O_2$ support material for Pt-based catalyst and was successfully applied in the oxygen reduction reaction (ORR) [20,21]. Due to their enhanced CO tolerance Pt/WO_x electrocatalysts have been considered as potential candidates for the PEMFC anode [22,23]. The incorporation of WO_3 into the Pt/C system also resulted in increasing ORR activity [24]. Furthermore, on account of the so called “spillover effect” tungsten oxides improve the catalytic activity in the hydrogen oxidation reaction (HOR) as well [25,26].

It is known that the resistance of the non-noble component against leaching at high

potentials is expected to be improved by incorporating tungsten or molybdenum into the TiO_2 lattice. The leaching can not only decrease activity and CO tolerance of the catalysts but also results in reduced electrolyte performance due to metal encapsulation in the membrane. In our recent studies [27,28] stabilization of W was achieved by isovalent substitution into the rutile-TiO_2 lattice, while the conductivity and corrosion resistance was ensured by a Ti-W mixed oxide - activated carbon composite type structure. A new multistep sol-gel synthesis method optimized for the preparation of $Ti_{0.7}W_{0.3}O_2$-C composites with mixed oxide and carbon in weight percent ratio 50:50 and almost exclusive tungsten incorporation into the rutile lattice was developed in these studies.

A further step in understanding of the doped TiO_2-carbon composite supports is to analyze the effect of the co-existence of the mixed oxide phase with non-incorporated fractions of the dopant material on the electrochemical performance, especially on the short-term stability, which gives information about the sensitivity for initial leaching. Accordingly, in this contribution the short-term stability of three $Ti_{(1-x)}W_xO_2$-C (x= 0.3-0.4) composite supports for Pt-based electrocatalysts with different tungsten incorporation are compared. The performance of these catalysts in the HOR is also tested. Based on our first results, the synthesis route of the $Ti_{0.7}Mo_{0.3}O_2$-C composite supports is described, which allows the comparison of the influence of various oxophilic doping metals (W and Mo) on the electrocatalytic performance. Finally, the promising electrochemical results obtained for the $Pt/Ti_{(1-x)}M_xO_2$-C (M=W, Mo) electrocatalysts are completed by single fuel cell test measurements carried out in pure hydrogen and under simulated CO poisoning conditions using 100 ppm CO/H_2 mixture to demonstrate the excellent CO tolerance of the novel catalysts.

2. Materials and methods

2.1. Synthesis of $Ti_{(1-x)}M_xO_2$-C (M= W, Mo; x= 0.3 - 0.4) composite materials and Pt electrocatalysts

Composite materials have been prepared by using sol-gel-based multistep synthesis routes ***A*** and ***B***, as shown in Fig 1. In both synthesis routes titanium-isopropoxide ($Ti(O\text{-}i\text{-}Pr)_4$, Aldrich, 97%) has been used as Ti precursor compound. Ammonium metatungstate hydrate ($(NH_4)_6H_2W_{12}O_{40}$, Fluka, 99%) and ammonium heptamolybdate tetrahydrate ($(NH_4)_6Mo_7O_{24}$ x $4H_2O$, Merck, 99%) were used as tungsten and molybdenum precursor compounds. The main difference between the routes is the order of the addition of the dopant precursor and the activated carbon (CABOT, Black Pearls 2000): in route ***A*** first rutile nuclei are formed on the

carbon then the dopant is introduced while in route ***B*** carbon is added to an aged colloidal solution containing both Ti and W ions. Detailed description of the synthesis procedure of $Ti_{0.7}W_{0.3}O_2$-C used in route ***A*** and its optimization can be found in [27]; for some details see also the Supplementary material.

The obtained $Ti_{(1-x)}W_xO_2$-C powders have been submitted to a high-temperature treatment (HTT) in He at 750°C for 8 h and reduction at 650°C for 10 min [27]. In case of $Ti_{0.7}Mo_{0.3}O_2$-C composites the final temperature of the HTT in argon atmosphere was decreased to 600ºC and reduction step was omitted (Fig. 1).

Route *A*

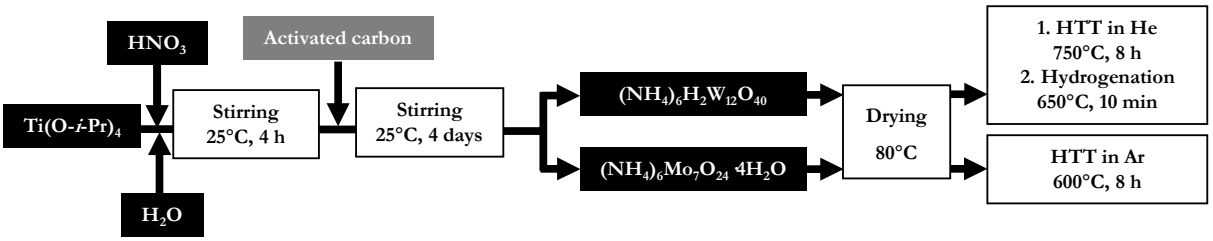

Route *B*

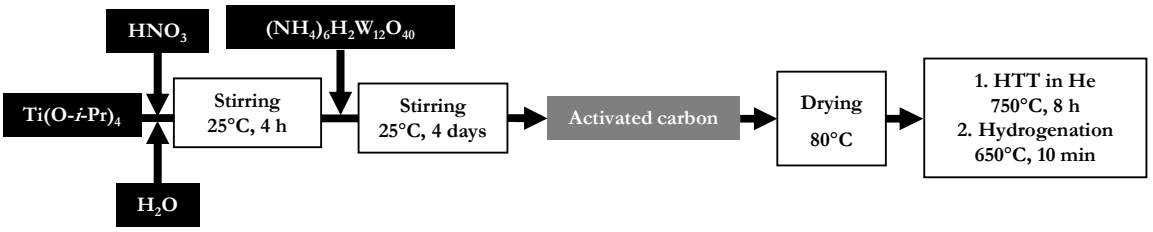

Fig. 1. Flow chart for preparing $Ti_{(1-x)}M_xO_2$-C (M= W, Mo) composite materials by using multistep synthesis routes ***A*** and ***B***.

Table 1 reports data on the actual composition and structure of the $Ti_{(1-x)}M_xO_2$-C (M= W, Mo; x= 0.3-0.4) composite materials. The sample identifier contains the intended composition of a $Ti_{(1-x)}M_xO_2$ mixed oxide reflecting the desired Ti/M atomic ratio; in all cases the mass ratio of the mixed oxide to the activated carbon was 50:50 (denoted as $Ti_{(1-x)}M_xO_2$-C).

Table 1. Structural properties of the $Ti_{(1-x)}M_xO_2$ (M= W, Mo; x= 0.3 - 0.4) composites and related Pt catalysts determined by XRD and TEM analysis.

Number [a]	Samples [b]	WHTT [c] (Phase, %)			HTT [d] (Phase, %)			Lattice parameters, Å [e]	M subst., %	Size, nm [f] (TEM)	
		R	A	MO_3/MO_2	R	A	MO_3/MO_2			before	after
1-W-A	$Ti_{0.7}W_{0.3}O_2$-C	100	0	0/0	92	0	0/8	*a*=4.670, *c*= 2.920	25-30	2.4±0.9	2.6±0.8
2-W-A	$Ti_{0.6}W_{0.4}O_2$-C	95	0	0/5	70	0	0/30	*a*=4.650, *c*= 2.930	20	3.5±1.1	3.1±0.9
3-W-B	$Ti_{0.7}W_{0.3}O_2$-C	0	100	0/0	0	70	0/30	-	-	2.8±0.9	3.2±1.0
1-Mo-A	$Ti_{0.7}Mo_{0.3}O_2$-C	100	0	0/0	95	0	0/5	*a*=4.670, *c*= 2.920	25-30	3.1±0.8	3.7±1.0

[a] ***A*** or ***B*** letter used in denomination of the samples indicates the synthesis route;

[b] Expected composition of mixed oxide reflects desired Ti/M atomic ratio;

[c] WHTT: the samples were studied without HTT;

[d] Detailed description of the HTT applied for W and Mo containing samples was shown in Fig. 1;

[e] Lattice parameters of the rutile phase obtained after HTT;

[f] Pt particles size measured on fresh catalysts and after the "pre-leaching" procedure.

R: rutile, A: anatase.

Pt loading from H_2PtCl_6 precursor was achieved using $NaBH_4$ and ethylene glycol (EG) [29] (for details see Supplementary Material); the platinum content was 40 wt% [27]. Commercially available standard 40 wt% Pt/C (Quintech (Q), C-40-Pt) and PtRu/C (Quintech, C-20-/10-Pt/Ru, Pt= 20 wt%, Ru= 10 wt% on Vulcan) electrocatalysts were used as a references.

2.2. Physical characterization

The composite supports were studied by powder X-ray diffraction (XRD) for determination of the crystalline phases and their cell parameters using a Philips model PW 3710 based PW 1050 Bragg-Brentano parafocusing goniometer with CuK_α radiation (λ= 0.15418 nm), graphite monochromator and proportional counter.

Transmission Electron Microscopy (TEM) studies of the samples were made by use of a FEI Morgagni 268D type transmission electron microscope.

Temperature Programmed Reduction (TPR) experiments were carried out in a commercial equipment (ASDI RXM 100- Advanced Scientific Designs Inc.) with a quartz flow reactor and a calibrated thermal conductivity detector.

Formation of the $Ti_{0.7}Mo_{0.3}O_2$-C composite during annealing was followed by X-ray photoelectron spectroscopy (XPS) measurements using an EA125 electron spectrometer (OMICRON Nanotechnology GmbH, Germany) with MgKα (1253.6 eV) excitation. Data were processed using the CasaXPS [30] and the XPS MultiQuant [31,32] software packages. Binding energies were referenced to the main component of the C 1s spectrum of the support (graphite at 284.4 eV binding energy).

Further details of the characterization by XRD, TEM, TPR and XPS techniques are given in the Supplementary Material.

2.3. Electrochemical characterization

$Pt/Ti_{(1-x)}M_xO_2$-C electrocatalysts were investigated by means of cyclic voltammetry and CO_{ad} stripping technique in conventional three-electrode electrochemical glass cell using a Biologic SP150 potentiostat. The most important information on the electrochemical measurements is summarized below; further details are given in the Supplementary Material.

The working electrode was prepared dipping a drop (3.6 μl) of catalyst ink on a freshly polished glassy carbon (GC) electrode (d = 0.3 cm, geometric surface area A= 0.0707 cm^2), and air-dry at room temperature (RT) for 30 minutes.

For the catalyst ink 5 mg catalyst sample was suspended in 4 ml H_2O (18.2 MΩ cm) + 1 ml isopropanol (Molar Chemicals, 99.5%) + 20 μl Nafion solution (D520 Nafion Dispersion, DuPont™ Nafion®). Pt loading of the electrodes was 20 μg cm^{-2}. The applied electrolyte was 0.5 M H_2SO_4 (Merck, P.A., 96%). The reference electrode was a hydrogen electrode immersed in the same electrolyte as the working electrode and all potentials are given on the RHE scale. Pt wire was used as a counter electrode.

In order to get information on the initial behavior of the electrocatalysts, CO_{ads} stripping voltammetry measurements were carried out on the samples without any electrochemical pre-conditioning or cleaning, and after the so-called "pre-leaching" treatment. Prior to the measurements gaseous CO was fed into the cell for 30 min while maintaining a constant potential of 50 mV. After CO removal (argon purge for 30 min), the working electrode was subjected to a cyclic voltammetry step at a 10 mV s^{-1} scan rate between 50 and 1000 mV. After the first CO stripping measurements the electrode was subjected to the "pre-leaching" procedure, by cyclic polarization with 50 mV s^{-1} for 35 cycles in the potential window between 50 and 1000 mV. Then the above described CO stripping measurement was repeated. After the second CO_{ads} stripping measurement the cyclic voltammogram (CV) was recorded again.

Catalytic activity in the HOR was tested by rotating disk electrode (RDE) technique in hydrogen saturated 0.5 M H_2SO_4 solution using a PAR 283 potentiostat. Pure and 100 ppm CO containing H_2 were used. GC electrode of 5 mm diameter (geometric surface area: 0.196 cm^2) was rotated at 225 rpm. 10 μl catalyst ink was dropped on the freshly polished GC electrode which resulted in about 20 μg cm^{-2} Pt loading.

2.4. Electrochemical single cell measurements

Fuel cell polarization measurements were carried out using Bio-Logic and Paxitech FCT-150S test device. Membrane electrode assemblies (MEAs) with catalyst coated gas diffusion layer and geometric area of 16 cm^2 were prepared by screen printing method. Gas diffusion electrodes were prepared using Teflon loaded carbon paper (H23C6, Freudenberg FCCT).

In all measurements commercial 40 wt% Pt/C (Q) catalyst was used as cathode. The metal loading in both electrodes was 0.4 mg_{Pt} cm^{-2}. The catalysts were suspended and ultrasonically mixed in EG, isopropanol and 5 % Nafion solution. The catalyst loading procedure was repeated two or three times, followed by drying in vacuum at 110°C for 12 hours.

MEAs were assembled by hot pressing the anode and cathode catalyst coated electrodes onto each side of a proton-conducting Nafion membrane (Nafion XL, Ion Power) using manual hydraulic press with heated platens (Specac Inc.) at 120°C under 57.3 kg cm^{-2} for 3 minutes.

Prior polarization measurements at 85±4ºC the MEA was activated at 0.6 V until the current stabilized (4-5 hours). The flow of gases was 120 ml min^{-1}; the gas pressure was 2 bar; the relative humidity for oxygen and hydrogen was 82 %. The polarization curves were obtained by measuring the voltage using stepwise increments of current density, at intervals of 12.5 mA cm^{-2} after 10 s at each point. The poisoning resistance of our catalyst was studied using 100 ppm CO/H_2 mixture. Further details are given in the Supplementary Material.

3. Results and discussion

3.1. Characterization of the $Ti_{(1-x)}W_xO_2$-C composite materials and related Pt catalysts

The structure of $Ti_{(1-x)}M_xO_2$-C (M= W, Mo) composites prepared by synthesis routes ***A*** and ***B*** was investigated by XRD measurements (see Table 1). Fig. 2 shows the XRD patterns of three W-based $Ti_{(1-x)}W_xO_2$-C composites obtained after the multistep HTT.

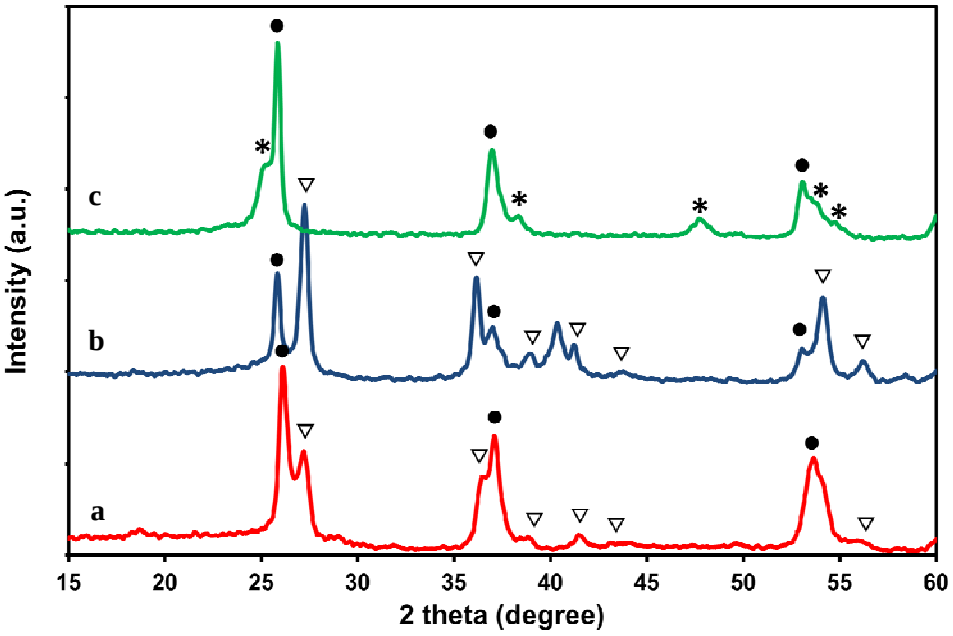

Fig. 2. XRD patterns of $Ti_{(1-x)}W_xO_2$-C composite materials after HTT in He and reduction: (a) 2-W-A sample, (b) 1-W-A sample, and (c) 3-W-B (composition of samples see in Table 1). ∇- Rutile, ∗ - anatase, ● - WO_2.

It has been demonstrated in our previous study [27,28] that preliminary formation of the rutile-TiO_2 phase in the presence of carbon at RT is prerequisite for complete W incorporation into the rutile lattice upon reduction at 650°C. XPS measurements confirmed that the incorporated tungsten was predominantly in the oxidation state of +4 [27,28]. Synthesis route ***A*** (Fig. 1), which is based on the incorporation of W or Mo into the pre-formed rutile-TiO_2-C composite, follows this pathway. Accordingly, upon the preparation of novel W- or Mo-containing composite materials the main tasks are (i) the formation of $Ti_{(1-x)}M_xO_2$ rutile phase with high crystallinity in the presence of carbon and (ii) the transformation of oxophilic M metal into oxidation state of four. It is necessary to mention that upon catalyst supports preparation increased stability and corrosion resistance of catalysts can be ensured by perfect coverage of carbon support with the mixed oxide layer.

The XRD technique was used to estimate the phase composition of the materials and determine the lattice parameters (Table 1). The computer modeling of a $Ti_{(1-x)}W_xO_2$ mixed oxide revealed [33] that upon tungsten incorporation into the rutile lattice the unit cell parameters and volume changes significantly. Therefore the lattice distortion can be used as an indicator of the tungsten incorporation. An expansion of the *a*-axis and a contraction of the *c*-axis are found and the maximum content of W, which can be reached upon incorporation into the rutile lattice, is 46 atomic percent ($Ti_{0.54}W_{0.46}O_2$). Based on these results, the $Ti_{0.6}W_{0.4}O_2$-C composite with desired Ti/W ratio of 0.6/0.4 (sample 2-W-A in Table 1) is very close to the incorporation limit for W, thus relatively big amount of free WO_2 phase may be expected, while sample 1-W-A ($Ti_{0.7}W_{0.3}O_2$-C) shows high level of tungsten incorporation into the rutile lattice.

In synthesis route ***B***, first carbon-free Ti-W mixed sol was prepared and then, after 4 days RT aging, activated carbon was introduced (Fig. 1). Based on the XRD results (sample 3-W-B in Table 1), after reduction in H_2 segregation of anatase-TiO_2 and WO_2 phases was observed.

According to the XRD results presented in Fig. 2 and Table 1, correlations were found between the experimental conditions, mainly the used preparation method (***A*** or ***B***), the ratio between Ti and W precursor compounds applied in synthesis and the structural properties as (i) the rutile or anatase phase formation and (ii) presence or absence of WO_2 phase not incorporated into the rutile crystal-lattice.

Although samples 2-W-A and 3-W-B structurally strongly deviate from a system with perfect W incorporation, their electrochemical study allows the assessment of the influence of the free, non-incorporated WO_2 oxide phase located in close proximity to either rutile-TiO_2

with partial W incorporation (sample 2-W-A in Table 1) or anatase-TiO_2 (sample 3-W-B in Table 1) on the CO tolerance, hydrogen spillover effect and stability of the electrocatalyst.

All Pt/$Ti_{(1-x)}W_xO_2$-C electrocatalysts prepared by loading of 40 wt% Pt were analyzed by TEM (see Table 1). In accordance with our earlier observations [27,28] results presented in Table 1 show that using this preparation method the uniform distribution of highly dispersed Pt particles with particle size of about 2-3 nm can be obtained.

CVs of the Pt/$Ti_{(1-x)}W_xO_2$-C (x= 0.3-0.4) catalysts obtained at the very beginning of the potential cycling can be seen in Fig. 3.A.

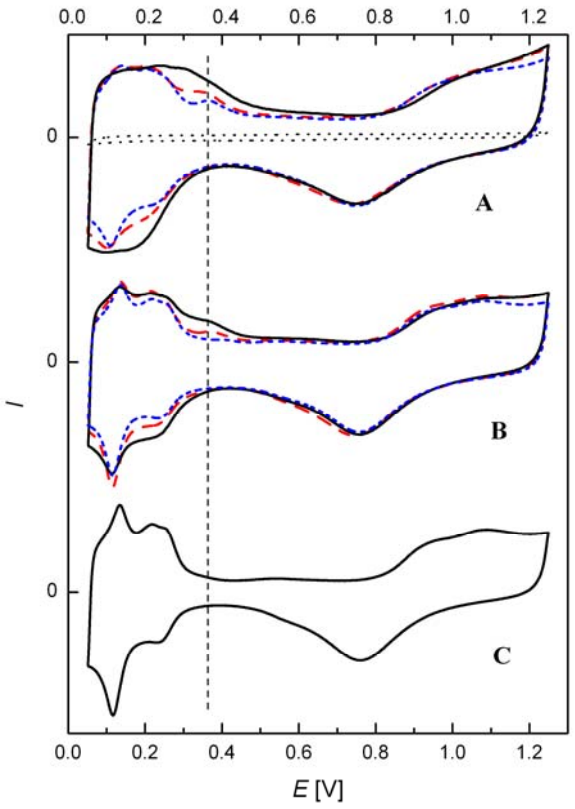

Fig. 3. Cyclic voltammograms of Pt/$Ti_{(1-x)}W_xO_2$-C catalysts in 0.5 M H_2SO_4. (A) 3rd cycle of a freshly prepared electrode: Pt/1-W-A (black solid line); Pt/3-W-B (red dash); Pt/2-W-A (blue short dash), CV of the bare composite support 1-W-A (black dotted line); (B) 20th cycle, (C) CV of the 40 wt% Pt/C (Q) catalyst.

Sweep rate: 100 mV s^{-1}. Current scale of the different catalysts was slightly balanced in order to enhance the visibility of the qualitative differences in the hydrogen adsorption/desorption region.

A characteristic feature of these voltammograms is the asymmetry in the so-called hydrogen region. All of the three samples show the same behavior irrespective of the preparation route or the composition of the samples, namely there is a more or less pronounced peak in the anodic branch of the voltammograms above 350 mV overlapping with the oxidation peak of the adsorbed hydrogen strongly bounded to the Pt surface.

The intensity of this peak slightly decreased with prolonged cyclic polarization as can be seen in Fig 3.B, and differences in the durability of this peculiarity among the investigated composite supports can be also observed. In the case of Pt/1-W-A sample after 20 potential cycles between 50 and 1250 mV there is still a distinct peak.

This voltammetric peak can not be assigned solely to the support, as can be seen from the voltammogram of the same amount of bare support (Fig 3.A) or to the platinum (Fig. 3.C shows a voltammogram of reference 40 wt% Pt/C (Q) catalyst), thus it can be the result of some collective effect of the support and the Pt.

Dependence of this peak on the potential limits of the cyclic polarization is demonstrated in Fig. 4.

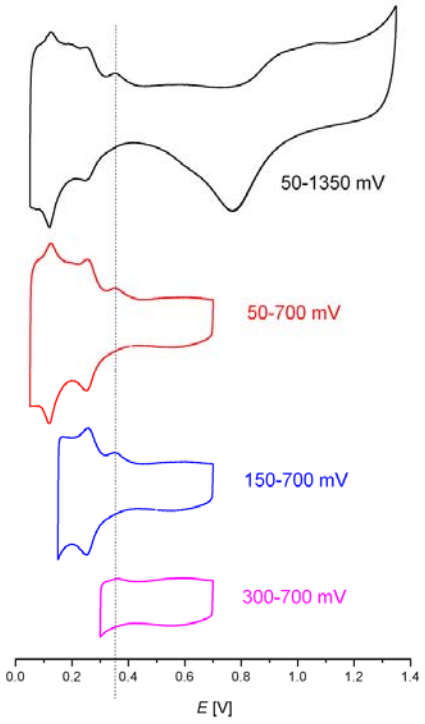

Fig. 4. Cyclic voltammograms of a Pt/1-W-A electrode in 0.5 M H_2SO_4 with different potential limits. Sweep rate: 20 mV s^{-1}; current scale is the same for all curves.

It was developed when the electrode previously had been polarized into the hydrogen adsorption region, but the anodic potential limit had no influence on the phenomenon. Furthermore, the peak could not be increased by holding the electrode potential in the hydrogen adsorption region for a longer period of time.

On the basis of these peculiarities, it seems reasonable to consider that the anodic peak being in question can be connected to the oxidation of tungsten bronze formed via the hydrogen spillover. Cathodic counterpart (i.e. the current peak of the formation of the tungsten bronze) of this anodic peak coincides with the hydrogen-adsorption peaks of the platinum. This assumption is supported by the facts that:

(i) it appears only when both Pt and mixed oxide support are present;

(ii) the amount of peak charge is structure sensitive, it depends on the support structure;

(iii) at the same time, the amount of the charge is limited, about 30 percent of the adsorbed hydrogen could be reached in the case of 1-W-A sample;

(iv) it appears when the electrode is polarized in the hydrogen adsorption region.

Similar appearance of the formation and oxidation of tungsten bronze on the voltammograms of different Pt-WO_x systems have been published earlier [13,34,35]. It is well-documented that atomic hydrogen can be reversibly stored in tungsten trioxide [36,37]. In acidic solutions H_{ad} produced on Pt surface can spillover to the surface of WO_3 to form hydrogen tungsten bronzes H_xWO_3 ($0.3<x<0.5$), which is an acid resistant metallic conductor [36]:

$$WO_3 + x\ Pt\text{-}H \rightarrow H_xWO_3 + x\ Pt \rightarrow WO_3 + x\ e^- + x\ H^+ + x\ Pt \qquad (1)$$

The proton conducting tungsten bronze also provides rapid hydrogen oxidation leading to the improvement of the overall catalytic activity [36,38]. Similar behavior was also reported for Pt-Mo system [39-43].

Fig. 5 compares the CVs and CO-stripping curves recorded on three W-containing Pt/$Ti_{(1-x)}W_xO_2$-C composite supported samples presented in Table 1. In this set of experiments CO_{ad} stripping was measured both on fresh catalysts and after the so-called ”pre-leaching” procedure in order to study the influence of the composite materials structure on the CO tolerance and short-term stability of the electrocatalysts. The influence of the”pre-leaching” on the Pt particle size was also studied by TEM. As shown in Table 1 all samples show quite good stability during cyclic polarization for 35 cycles in the potential window between 50 and 1000 mV.

It is well accepted in the literature [22,25,38,44-46] that the way for improving the CO tolerance of the electrocatalyst by the bifunctional mechanism is to create interfaces between Pt particles and an oxide-containing support, which is (i) stable under the reaction conditions, (ii) electroconductive, (iii) stabilizes the small size of the Pt nanoparticles and (iv) generates OH groups as oxidants at low potential. $Ti_{(1-x)}M_xO_2$-C (M= W, Mo) composites are good candidates for this role.

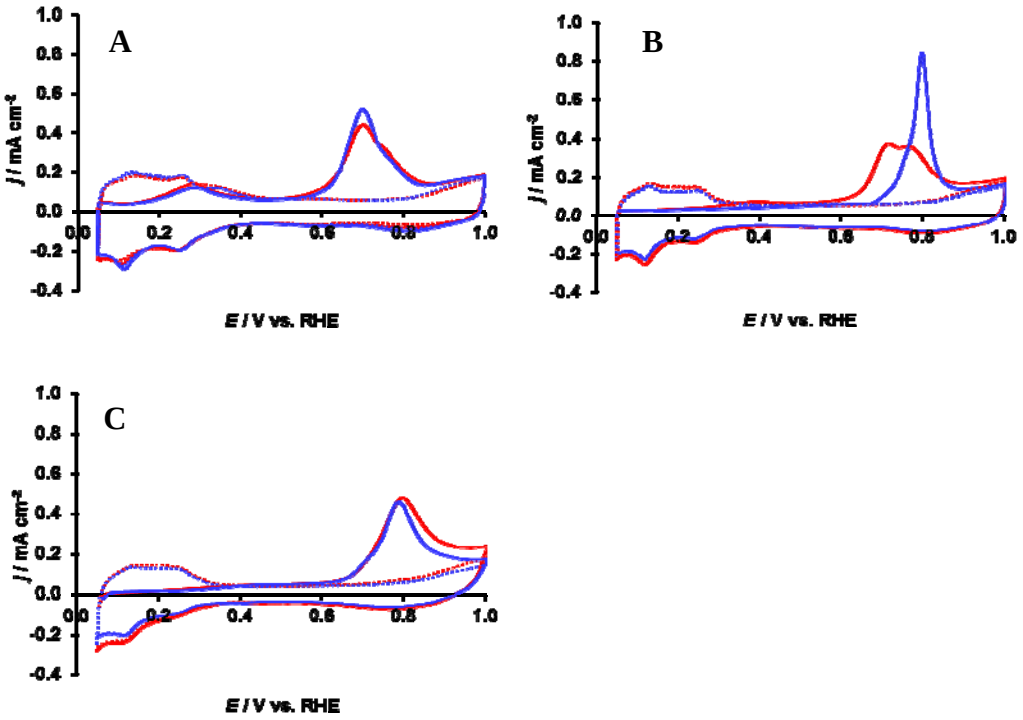

Fig. 5. Electrochemical stability and CO-tolerance study by cyclic polarization on fresh catalyst samples (1st cycle) and after the"pre-leaching" procedure (35th cycle) of platinum catalysts supported on (A) 1-W-A, (B) 2-W-A and (C) 3-W-B composites. 1st cycle: CO_{ads} stripping voltammograms (solid red lines) and CVs recorded after the CO oxidation cycle (dotted red lines); 35th cycle: CO_{ads} stripping voltammograms (solid blue lines) and CVs recorded after the CO oxidation cycle (dotted blue lines). Obtained in 0.5 M H_2SO_4 at 10 $mV \cdot s^{-1}$. The current was normalized to the geometric surface area.

At the moment, the nature of the oxygenated species provided by MO_x (M= W, Mo) is still unclear. The „active" oxygenated species are considered to be oxy-hydroxide groups (M-OH) of the MO_x support. It is also worth noting that surface hydroxylation of the MO_x surface is facilitated by exposure to the acidic electrolyte. For Pt/WO_x catalytic systems it has been

proposed that W-OH groups, formed upon H^+ insertion or by dissociative adsorption of water molecules, are involved in the electrooxidation of CO_{ads} species adsorbed on Pt sites [25]:

$$(–O–W–OH) + CO_{ads,\ Pt} \rightarrow (–O–W) + CO_2 + H^+ + e^- \qquad (2)$$

As emerges from Fig. 3.B after 20 potential cycles up to 1250 mV a pronounced redox tungsten peak at 350 mV was observed only on the Pt/1-W-A sample with good W incorporation. After CO admission in 1st and 35th cycles on this catalyst (Fig. 5.A) a "pre-peak" centered at 290 mV and the main peak at 700 mV with small shoulder at 760 mV were found. As presented in Fig. 5.A this catalyst shows high CO tolerance and stability after 35 potential cycles. The onset potential ($E_{CO,onset}$) for the oxidation of CO is 120 mV.

On catalyst prepared using 2-W-A support (consisting of co-existing W-doped rutile TiO_2 and non-incorporated WO_2, see Table 1 and Fig. 5.B) after 1st cycle of CO adsorption a small "pre-peak" appeared at about 370 mV followed by two CO_{ads} electrooxidation peaks at 705 and 760 mV. The $E_{CO,onset}$ is 200 mV. A similar double-peaked CO stripping voltammogram (with peaks at 710 and 780 mV) was reported for a Pt/$Ti_{0.7}W_{0.3}O_2$-C catalyst supported by a composite material with partial W incorporation in our recent study [27]. The presence of a small "pre-peak" between 400 and 700 mV followed by two peaks at 760 and 840 mV was demonstrated on Pt-WO_x/C catalysts in Ref. [44]. After 35 potential cycles the admission of CO (Fig. 5.B) results in pronounced change in CO_{ads} stripping voltammogram: the small "pre-peak" disappears and the main anodic peak shifts to ca. 795 mV; the voltammogram resembles that of usually characteristic for reference Pt/C catalyst. However, the $E_{CO,onset}$ value remains unchanged. Based on the literature results [44] the peak at 800 mV can be attributed to the CO oxidation on Pt nanoparticles weakly interacted with W-containing underlying layer. It can be proposed that the"pre-leaching" procedure on the Pt/2-W-A sample results in pronounced decrease the number of Pt sites at the interface with W-containing species, such as $Ti_{(1-x)}W_xO_2$ and/or WO_2.

As shown in Fig. 5.C, in case of the catalyst prepared using support containing segregated anatase-TiO_2 and WO_2 oxide phase (3-W-B sample in Table 1) one wide CO_{ads} electrooxidation peak with maximum at 785 mV was observed. The asymmetrical peak has small shoulder at about 715 mV. The characteristic redox "pre-peak" (if exist) is hardly detected. However, the $E_{CO,onset}$ for the oxidation of CO is even less than 200 mV. It is necessary to mention that prolonged cyclic polarization up to 1000 mV has no influence on the voltammogram shape, thus demonstrating stability of the catalyst during the "pre-leaching" procedure. According to Fig. 3 and Fig. S1 in the Supporting Material, however,

this stability is limited to a narrower potential range than in the case of the the Pt/1-W-A catalyst with high level of tungsten incorporation. The anodic peak connected to the oxidation of tungsten bronze rapidly disappears from the cyclic voltammogram of Pt/3-W-B under polarization up to 1250 mV but can be retained by lowering the upper potential limit to 1000 mV (Fig. S1).

As was mentioned above, the tolerance to CO of the WO_x-containing Pt-based catalysts at low electrode potentials likely proceeds by a bifunctional mechanism, and, consequently, the "active sites" are located at the Pt-WO_x interface. The lack of the "pre-peak" and the shift of the CO electrooxidation peak towards more positive potentials therefore may be attributed to imperfect covering of carbon particles with TiO_2 and/or WO_2 oxides for the composite materials prepared by using route ***B*** and decreased number of the Pt-WO_x "active sites".

Summarizing the findings presented in Fig. 5 it can be concluded that enhanced CO tolerance after "pre-leaching" procedure was observed only on the Pt/$Ti_{0.7}W_{0.3}O_2$-C catalyst with almost complete W incorporation. It is well-known that stability of tungsten against leaching at high potentials can be improved by incorporating tungsten into the TiO_2 lattice (H_xWO_y bronzes are not stable above E= 600 mV vs. RHE [25,47]). Accordingly, the leaching of WO_2 may be one of the reasons of activity and CO tolerance decrease observed on two samples containing rather big amount of oxide phase (see Table 1).

In Ref. [48] "pre-peak" centered at ca. 450 mV was attributed to the faradaic process of intercalation/de-intercalation of H atoms into MoO_y lattice. In accordance with experimental data presented for Pt/Ti_3O_5-Mo catalyst [48] the disappearance of the redox peak after 1000 cycles of cyclic polarization and decrease of the "pre-peak" intensity accompanied with simultaneous shift to higher potential in the CO stripping voltammograms were observed. Based on these observations and our results presented in Figs. 3 and 5 the correlation between the tolerance to CO and the presence or absence of the anodic peak, connected to the oxidation of H_xMO_y (M= W, Mo) bronze formed via the hydrogen spillover, can be proposed.

Increased CO-tolerance of the Pt catalysts as a result of the $Ti_{(1-x)}M_xO_2$-C composite support is also demonstrated by Fig. 6. Behavior of the catalysts in the HOR was tested in pure hydrogen and in the presence of the CO/H_2 mixture. Current vs. time curves were registered after a potential step from open circuit potential to 500 mV on rotating disc electrodes prepared from the Pt/1-W-A, Pt/3-W-B catalysts and from the reference Pt/C (Q). In the case of platinum metals this potential value is certainly in the diffusion limited range when pure hydrogen is oxidized. Thus, the behavior of the catalysts in pure hydrogen was very similar and for this reason only the curve for Pt/C is presented. Effect of CO can be seen

when the activity of the surface significantly decreases and the rate of HOR becomes kinetically controlled. 100 ppm CO contaminant in the hydrogen feed resulted in fast decrease of the HOR current in the case of the Pt/C (compare curves 1 and 2 in Fig. 6). Under the same circumstances on electrodes prepared from the Pt/1-W-A and Pt/3-W-B catalysts quite stable *I* vs. time curves could be obtained (curve 3 and 4 in Fig. 6).

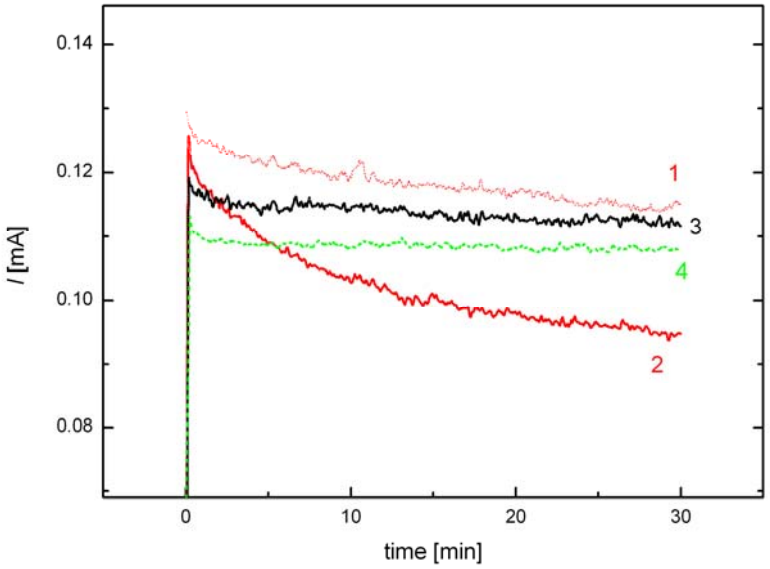

Fig. 6. HOR-current vs. time at 500 mV potential in hydrogen saturated 0.5 M H_2SO_4 solution on a RDE (at 225 rpm). 1: Pt/C (Q) in pure hydrogen, 2: Pt/C (Q), 3: Pt/1-W-A and 4: Pt/3-W-B catalysts in 100 ppm CO containing hydrogen.

To summarize the analysis of the effect of the structure of the support on the electrochemical performance of the W-doped composite supported catalysts, CV, CO stripping and HOR data demonstrate the good activity, CO tolerance and stability of the Pt/1-W-A catalyst with high level of W incorporation. Results for Pt/3-W-B with segregated anatase-TiO_2 and WO_2 indicate a narrower stability range but still good activity in HOR under the applied measurement parameters even in the presence of CO, thus tests under working conditions of a fuel cell are needed to clarify the role of W incorporation on the catalytic performance. The Pt/2-W-A with partially incorporated W turned out to be very unstable.

3.2. Characterization of the $Ti_{0.7}Mo_{0.3}O_2$-C composite and related Pt catalyst

As shown in Table 1 upon using the optimized preparation route ***A*** $Ti_{0.7}Mo_{0.3}O_2$-C composite was also successfully synthesized. The challenge in the preparation of

$Ti_{0.7}Mo_{0.3}O_2$-C composite materials with high degree of Mo incorporation is to achieve complete isovalent Mo incorporation into the rutile-TiO_2 lattice. The appropriate conditions for preparation of this material were selected based on TPR measurements and XPS controlled annealing experiments carried out *in situ* in the preparation chamber of the electron spectrometer.

According to TPR results (TPR profile not shown) the hydrogen consumed in the range ~220ºC ≤ T ≤ 700ºC was only slightly higher than the amount of H_2 required for the reduction of $Mo^{6+} \rightarrow Mo^{4+}$ and the maximum of the H_2 consumption observed at about 490ºC was shifted by ca. 150ºC to lower temperatures compared to the reduction of W containing composites. These results point to the easy reducibility of molybdenum.

The results of the XPS experiments are summarized in Figure 7, where the Mo 3d core level spectra are shown after different treatments.

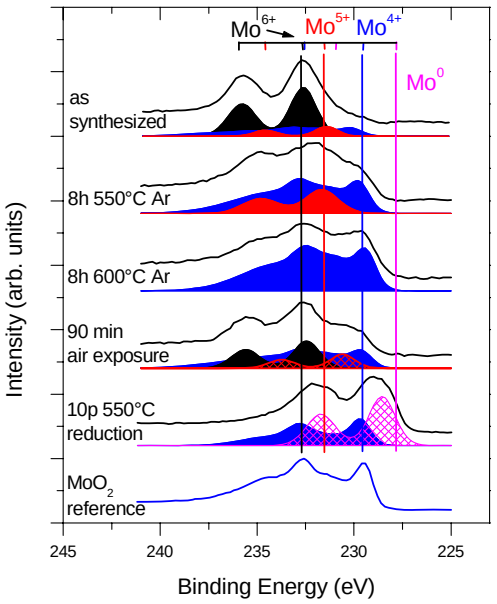

Fig. 7. Mo 3d XPS spectra of the $Ti_{0.7}Mo_{0.3}O_2$-C composite obtained after different *in situ* treatments.

After synthesis finished by annealing at 600°C in Ar the sample was stored in air. The Mo 3d spectrum of this sample contains a narrow spin-orbit splitted peak pair with the $3d_{5/2}$ component at 232.6 eV binding energy; this feature can be assigned to the Mo^{6+} ionic state [49]. At lower binding energies Mo^{5+} (231.4 eV) and Mo^{4+} contributions can be identified, which probably arise from molybdenum ions incorporated into the rutile lattice. After 8 h

annealing at 550°C in 100 mbar Ar the Mo 3d spectrum transforms into a broad and rather structureless feature; its smallest binding energy contribution is around 229.5 eV, which can be assigned to Mo^{4+} ions [49]. Further 8 h annealing at 600°C in Ar results in a spectrum which can be described as a combination of a narrower and a broad spin-orbit splitted doublet with the most intense contribution still at 229.4 eV. According to our own data (see the lowermost spectrum of Fig. 7) and the literature [50,51], this spectrum can be assigned to Mo^{4+} ions in MoO_2; the two peak pairs represent differently screened final states. A short reduction in 100 mbar H_2 for 10 min results in the appearance of an even smaller binding energy component around 228.5 eV, which, although is located at slightly higher binding energy than that of metallic Mo (228.0 eV), indicates partial reduction towards the metallic state [49]. Since metallic molybdenum is undesirable, one can conclude that the reduction step is unnecessary during the synthesis process. Exposure of the sample annealed in Ar (i.e. without reduction) to air leads to partial re-oxidation of Mo, involving the appearance of the 6+ ionic state, while a certain part still maintains its 4+ oxidation state. According to these XPS results upon preparation of Mo-containing composites the reduction step was omitted.

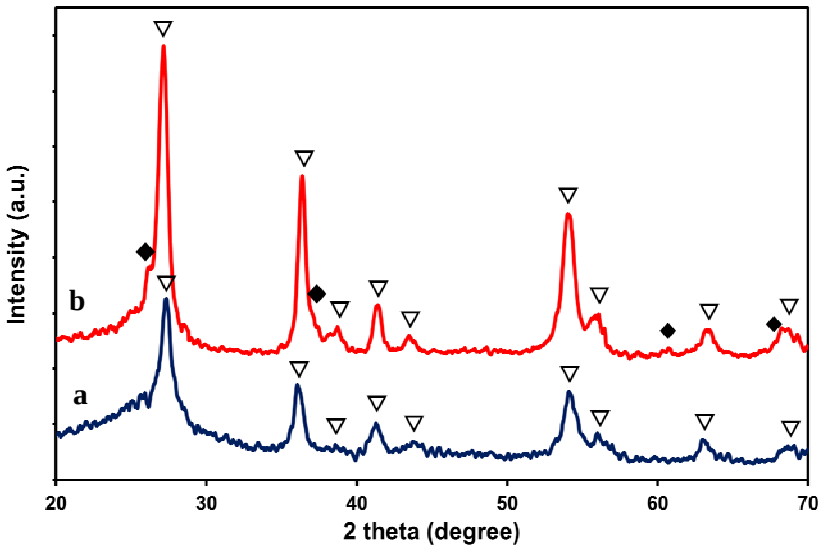

Fig. 8. XRD patterns of $Ti_{0.7}Mo_{0.3}O_2$-C composite before (a) and after HTT (b). ∇- Rutile, ◆ - MoO_2.

Fig. 8 shows the XRD patterns of $Ti_{0.7}Mo_{0.3}O_2$-C composite obtained before and after the HTT. The powder obtained before any HTT consists of rutile crystallites (Fig. 8, sample **a**). After the heat treatment in Ar at 600°C for 8 h (Fig. 8, sample **b**) almost pure rutile phase was obtained (R/MoO_2= 95/5) with high degree of Mo incorporation (Mo_{subst}= 25-30 %). The

changes in the lattice parameters (a= 4.670 Å, c= 2.920 Å, while pure rutile TiO_2 structure has a= 4.593 Å, c= 2.959 Å) confirm the presence of molybdenum incorporated into the unit cell (see Table 1).

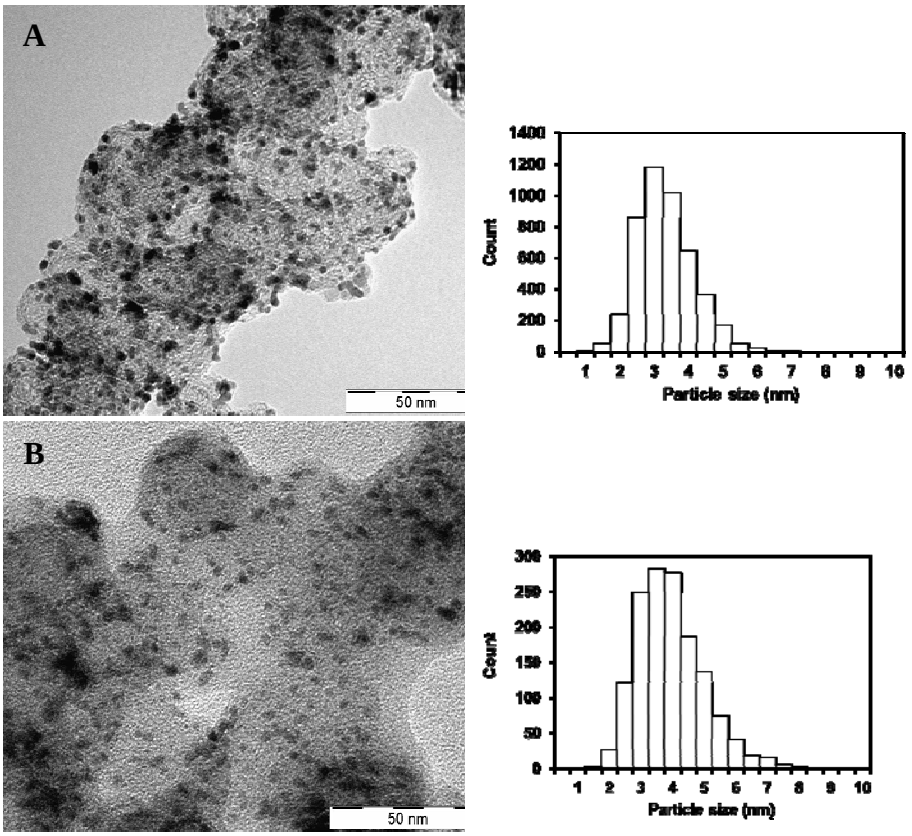

Fig. 9. TEM images and histogram of particle size distribution for the $Pt/Ti_{0.7}Mo_{0.3}O_2$-C electrocatalyst before (A) and after the "pre-leaching" experiment (B).

TEM micrographs of the 40 wt% $Pt/Ti_{0.7}Mo_{0.3}O_2$-C sample obtained both on fresh catalyst and after the "pre-leaching" procedure along with the corresponding histogram for particle size distribution are presented in Fig. 9. As seen from the data given in Table 1, this catalyst shows good stability during short-term cyclic polarization. Fig. 9 reveals the narrow distribution of the Pt particles both for fresh samples and those after the "pre-leaching" test with mean particle size of 3.1 ± 0.8 nm and 3.7±1.0 nm, respectively.

As shown in Fig. 10 CO_{ad} stripping voltammograms were measured both on fresh catalyst and after the "pre-leaching" test performed by cyclic polarization for 35 cycles. A typical CV of Pt with the classical features of the under-potentially deposited hydrogen adsorption/desorption between $0.05 < E < 0.40$ V along with a redox peak between 380 and 530 mV was observed on $Pt/Ti_{0.7}Mo_{0.3}O_2$-C sample presented in Fig. 10.

The CO stripping voltammogram for the $Pt/Ti_{0.7}Mo_{0.3}O_2$-C catalyst displays two clear oxidation features: (i) the main anodic peak at 705 mV, and (ii), two small overlapping "pre-peaks" centered at ca. 215 and 400 mV, due to the oxidation of weakly bonded CO. It has been demonstrated by Differential Electrochemical Mass Spectrometry that both peaks are related to the CO_2 production [52,53]. As was previously mentioned, the early onset of CO oxidation as a "pre-peak" is typical for Pt-based catalysts containing Ti, Ta, W, and Mo suboxides [53,54].

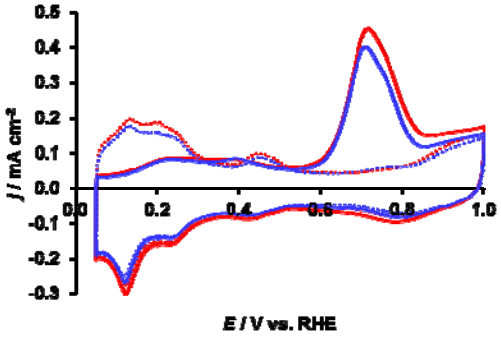

Fig. 10. Electrochemical stability and CO-tolerance study by cyclic polarization on fresh $Pt/Ti_{0.7}Mo_{0.3}O_2$-C catalyst sample (1st cycle) and after "pre-leaching" test (35th cycle). 1st cycle: CO_{ads} stripping voltammograms (solid red lines) and CVs recorded after the CO oxidation cycle (dotted red lines); 35th cycle: CO_{ads} stripping voltammograms (solid blue lines) and CVs recorded after the CO oxidation cycle (dotted blue lines). Obtained in 0.5 M H_2SO_4 at 10 $mV \cdot s^{-1}$. The current was normalized to the geometric surface area.

We reported earlier that on the 40 wt% Pt/C catalyst the main CO_{ads} stripping peak was observed at ca. 820 mV [27,28]. The position of this peak is shifted towards positive potentials by 115 mV with respect to the main peak observed on the Pt/1-Mo-A sample, thus demonstrating increased tolerance to CO. Results presented in Fig. 10 show that the position and intensity of peaks was only slightly affected by the aging procedure applied. It is necessary to mention that both Pt-based catalysts supported on $Ti_{(1-x)}M_xO_2$-C composites with good incorporation of oxophilic doping W and Mo metals (samples 1-W-A and 1-Mo-A in Table 1) showed quite similar behavior during electrochemical experiments evidencing increased CO tolerance and stability during 35 polarization cycles. We believe this similarity is due to the similar nature of the hydroxyl groups provided by the W- or Mo-doped mixed

oxide support for CO oxidation by the bifunctional mechanism, while the enhanced stability is due to the protective effect of the mixed oxide against dissolution in both cases.

3.3. Characterization in a single cell test device

The electrochemical activity and CO-tolerance of the Pt/1-W-A, Pt/3-W-B and Pt/1-Mo-A catalysts were also studied by measurements in a fuel cell test device in comparison with commercial Pt/C and PtRu/C catalysts from Quintech. As shown in Fig. 11.A the polarization curves for pure H_2 are practically the same for all investigated samples with cell potential of about 600-630 mV at 1 A cm^{-2}.

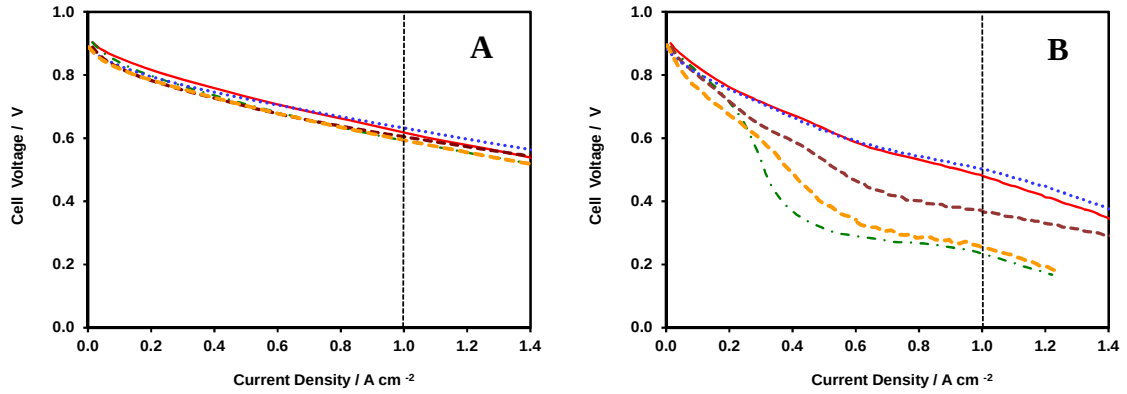

Fig. 11. Cell potential vs. current density plots for single cells with pure H_2 (A) and 100 ppm CO/H_2 fuel (B): Pt/1-W-A (straight red line), Pt/1-Mo-A (dotted blue line), Pt/3-W-B (dashed orange line) and Pt/C (green line)). The state-of-the art CO-tolerant PtRu/C electrocatalyst (Q) was given for comparison (dashed brown line).

Considering that the composite support contains a phase with relatively low conductance, it may seem surprising that the overall ohmic losses are essentially the same in cells using either pure carbon or mixed oxide-carbon composite supported catalysts. The general fuel cell literature attributes these losses to (i) proton conduction through the membrane and (ii) limited conductivity of current paths from the surface of the electrode to the bipolar plates. The latter combines contributions from the bulk conductance of the bipolar plates and the materials of the gas diffusion layers as well as from the conductance of the contacts between the electrocatalyst, the gas diffusion layer and the bipolar plate.

Considering the high specific surface area of the Black Pearls 2000 carbon used in this study (S_{BET}= 1475 m^2 g^{-1}), complete and uniform coverage by the mixed oxide is unlikely.

Thus a percolating network of carbon-carbon contacts is expected to exist in the composite supported electrocatalyst, which results in conductivity close to that of the unmodified carbon (2.2 S cm^{-1} [55]) as confirmed by our preliminary measurements and literature examples [56,57]. Accordingly, the conductance of the carbon-carbon contacts determines the ohmic losses both within the electrocatalyst layer and at the electrocatalyst/gas diffusion layer interface, and not much variation is expected regardless if the composite catalysts or the pure carbon supported references are used.

Moreover, in Ref. [5] it has been demonstrated that the performance of a (carbon-free, insulating) Pt/TiO_2 electrocatalyst in a fuel cell was comparable to that of commercial Pt/C. This result further confirms that the effect of the conductance of the electrocatalyst on the internal resistance of the cell is small.

The results obtained for the Pt/1-W-A and the Pt/1-Mo-A catalysts using hydrogen containing 100 ppm CO show that the performance is much better than for commercial Pt/C (Q) catalyst (see Fig. 11.B): the voltage loss with respect to the pure H_2 fuel is 130-140 mV for both composite supported catalysts, while in the case of the Pt/C catalyst it is 360 mV. Similar good results have been reported for $Pt_{0.8}Mo_{0.2}$ alloy nanoparticles [58] and Pt-M/C (M= Mo and W) electrocatalysts prepared using formic acid reduction method [59]. It is necessary to mention that the state-of-art CO tolerant PtRu/C (Q) benchmark catalyst showed slightly lower performance (230 mV voltage loss was observed at 1 A cm^{-2}) than our two composite supported Pt catalysts. On the other hand, the Pt/3-W-B catalyst with segregated anatase and WO_2 in the support behaves similarly to the Pt/C reference exhibiting clear signs of CO poisoning, which could not be detected by the rotating disc electrode measurement. However, it is necessary to mention that the mass transport conditions in the rotating electrode HOR measurement and in the fuel cell are very different.

Conclusions

$Ti_{(1-x)}W_xO_2$-C (x= 0.3-0.4) composite materials were prepared using two different synthesis routes based on preliminary formation of (i) the rutile-TiO_2 phase in the presence of activated carbon, followed by W precursor addition (route ***A***) and (ii) Ti-W mixed sol, followed by active carbon addition (route ***B***). According to the XRD results correlations were found between the experimental conditions, mainly the used preparation method (***A*** or ***B***), the ratio between Ti and W precursor compounds and the structural properties.

Novel $Ti_{0.7}Mo_{0.3}O_2$-C composite with high level of isovalent Mo incorporation was obtained by route ***A***. Incorporated molybdenum was confirmed to be predominantly in the +4 oxidation state by XPS, in line with the TPR findings.

Comparison of the electrochemical properties of $Pt/Ti_{(1-x)}W_xO_2$-C catalysts prepared on supports with different structural characteristics confirmed that the CO tolerance is connected to the stability of the oxide-Pt interface. The degree of W incorporation was found to correlate with the hydrogen spillover effect and the short-term stability, which determine the activity of the catalyst and its suitability for use in fuel cells.

No significant difference in the activity, stability during 35 polarization cycles and CO tolerance was found between the tungsten- and molybdenum-containing $Ti_{0.7}M_{0.3}O_2$-C composite supported Pt catalysts, if the oxophilic doping metals were completely incorporated. At the same time, better performance of the $Pt/Ti_{0.7}M_{0.3}O_2$-C (M= W, Mo) electrocatalysts in a single cell test device using hydrogen containing 100 ppm CO compared to the reference Pt/C and PtRu/C (Q) catalysts was also demonstrated.

Acknowledgements

This work was supported by the National Development Agency [grant number KTIA_AIK_12-1-2012-0014]. Financial support by the OTKA-project [grant numbers K100793 (Zoltán Pászti) and K112034 (István Bakos)] is greatly acknowledged.

References

[1] Meier JC, Galeano C, Katsounaros I, Topalov AA, Kostka A, Schuüth F, Mayrhofer KJJ. Degradation Mechanisms of Pt/C Fuel Cell Catalysts under Simulated Start-Stop Conditions. ACS Catal 2012; 2: 832-843.

[2] Mathias MF, Makharia R, Gasteiger HA, Conley JJ, Fuller TJ, Gittleman CI, Kocha SS, Miller DP, Mittelsteadt CK, Xie T, Yan SG, Yu PT. Two Fuel Cell cars in every garage? Electrochem Soc Interface 2005;14:24-35.

[3] Subban C, Zhou Q, Leonard B, Ranjan C, Edvenson HM, DiSalvo FJ, Munie S, Hunting J: Catalyst supports for polymer electrolyte fuel cells. Phil Trans R Soc A 2010;368:3243-3253.

[4] Huang SY, Ganesan P, Popov BN. Electrocatalytic activity and stability of titania-Supported Platinum-Palladium electrocatalysts for Polymer Electrolyte Membrane Fuel Cell. ACS Catal 2012;2:825-831.

[5] Huang SY, Ganesan P, Popov BN. Development of a Titanium Dioxide-Supported

Platinum Catalyst with Ultrahigh Stability for Polymer Electrolyte Membrane Fuel Cell Applications. J Am Chem Soc 2009;131:13898-13899.
[6] Rajesh B, Thampi KR, Bonard JM, Mathieu HJ, Xanthopoulos N, Viswanathan B. Electronically conducting hybrid material as high performance catalyst support for electrocatalytic application. J Power Sources 205;141:35-38.
[7] Chhina H, Campbell S, Kesler O. An oxidation-resistant indium tin oxide catalyst support for proton exchange membrane fuel cells. J Power Sources 2006;161:893-900.
[8] Huang SY, Ganesan P, Popov BN. Titania supported platinum catalyst with high electrocatalytic activity and stability for polymer electrolyte membrane fuel cell. Appl Catal B Environ 2011;102:71-77.
[9] Hakamizadeh M, Afshar S, Tadjarodi A, Khajavian R, Fadaie MR, Bozorgi B. Improving hydrogen production via water splitting over Pt/TiO_2/activated carbon nanocomposite. Int J Hydrogen Energy 2014;39:7262-7269.
[10] N. Rajalakshmi N, N. Lakshmi N, K.S. Dhathathreyan KS. Nano titanium oxide catalyst support for proton exchange membrane fuel cells. Int J Hydrogen Energy 2008;33:7521-7526.
[11] Grätzel M. Photoelectrochemical cell. Nature 2001;414:338-344.
[12] Fujishima A, Honda K. Electrochemical Photolysis of Water at a Semiconductor Electrode. Nature 1972;238:37-38.
[13] Wang D, Subban CV, Wang H, Rus E, DiSalvo FJ, Abruña HD. Highly Stable and CO-Tolerant Pt/$Ti_{0.7}W_{0.3}O_2$ Electrocatalyst for Proton-Exchange Membrane Fuel Cells. J Am Chem Soc 2010;132:10218-10220.
[14] Chevallier L, Bauer A, Cavaliere S, Hui R, Rozière J, Jones DJ. Mesoporous Nanostructured Nb-Doped Titanium Dioxide Microsphere Catalyst Supports for PEM Fuel Cell Electrodes. ACS Appl Mater Interfaces 2012;4:1752-1759.
[15] Elezović NR, Babić BM, Gajić-Krstajić Lj, Radmilović V, Krstajić NV, Vračar LJ. Synthesis, characterization and electrocatalytical behavior of Nb-TiO_2/Pt nanocatalyst for oxygen reduction reaction. J Power Sources 2010;195:3961- 3968.
[16] Do TB, Cai M, Ruthkosky MS, Moylan TE. Niobium-doped titanium oxide for fuel cell application. Electrochim Acta 2010;55:8013-8017.
[17] Kumar A, Ramani V. $Ta_{0.3}Ti_{0.7}O_2$ Electrocatalyst Supports Exhibit Exceptional Electrochemical Stability. J Electrochem Soc 2013;160:F1207-F1215.
[18] Subban CV, Zhou Q, Hu A, Moylan TE, Wagner FT, DiSalvo FJ. Sol-Gel Synthesis, Electrochemical Characterization, and Stability Testing of $Ti_{0.7}W_{0.3}O_2$ Nanoparticles for Catalyst Support Applications in Proton-Exchange Membrane Fuel Cells. J Am Chem Soc

2010;132:17531-17536.

[19] Odetola C, Easton EB, Trevani L. Investigation of TiO_2/carbon electrocatalyst supports prepared using glucose as a modifier. Int J Hydrogen Energy 2016;41:8199-8208.

[20] Ho VTT, Pan CJ, Rick J, Su WN, Hwang BJ. Nanostructured $Ti_{0.7}Mo_{0.3}O_2$ Support Enhances Electron Transfer to Pt: High-Performance Catalyst for Oxygen Reduction Reaction. J Am Chem Soc 2011;133:11716-11724.

[21] Nguyen TT, Ho VTT, Pan CJ, Liu JY, Chou HL, Rick J, Su WN, Hwang BJ Synthesis of $Ti_{0.7}Mo_{0.3}O_2$ supported- Pt nanodendrites and their catalytic activity and stability for oxygen reduction reaction. Appl Catal B Environ 2014;154-155:183-189.

[22] Pereira LGS, dos Santos FR, Pereira ME, Paganin VA, Ticianelli EA. CO tolerance effects of tungsten-based PEMFC anodes. Electrochim Acta 2006;51:4061-4066.

[23] Micoud F, Maillard F, Gourgaud A, Chatenet M. Unique CO-tolerance of Pt-WO_x materials. Electrochem Commun 2009;11:651-654.

[24] Hernandez-Pichardo ML, Gonzalez-Huerta RG, del Angel P, Tufino-Velazquez M, Lartundo L. The role of the WO_3 nanostructures in the oxygen reduction reaction and PEM fuel cell performance on WO_3-Pt/C electrocatalysts. Int J Hydrogen Energy 2015;40:17371-17379.

[25] Micoud F, Maillard F, Bonnefont A, Job N, Chatenet M. The role of the support in CO_{ads} monolayer electrooxidation on Pt nanoparticles: Pt/WO_x vs. Pt/C. Phys Chem Chem Phys 2010;12:1182-1193.

[26] Tseung ACC, Chen KY. Hydrogen spill-over effect on Pt/WO_3 anode catalysts. Catal Today 1997;38:439-443.

[27] Gubán D, Borbáth I, Pászti Z, Sajó IE, Drotár E, Hegedűs M, Tompos A. Preparation and characterization of novel $Ti_{0.7}W_{0.3}O_2$-C composite materials for Pt-based anode electrocatalysts with enhanced CO tolerance. Appl Catal B Environ 2015;174:455-470.

[28] Gubán D, Pászti Z, Borbáth I, Bakos I, Drotár E, Sajó IE, Tompos A. Design and preparation of CO tolerant anode electrocatalysts for PEM fuel cells. Period Polytech- Chem 2016;60:29-39.

[29] Kim P, Joo JB, Kim W, Kim J, Song IK, Yi, J. $NaBH_4$-assisted ethylene glycol reduction for preparation of carbon-supported Pt catalyst for methanol electro-oxidation. J Power Sources 2006;160: 987-990.

[30] Fairley N. "CasaXPS: Spectrum Processing Software for XPS, AES and SIMS," Version 2.3.13, Casa Software Ltd, Cheshire. 2006. http://www.casaxps.com

[31] Mohai M. “XPS MultiQuant: Multimodel XPS Quantification Software,” Surface and Interface Analysis 36(8), pp. 828-832. 2004.

[32] Mohai M. “XPS MultiQuant: Multi-model X-ray photoelectron spectroscopy quantification program,” Version 3.00.16. 2003.

[33] Peters E, Mueller-Buschbaum H. Ueber ein niedervalentes Titan-Wolframoxid: $Ti_{0.54}W_{0.46}O_2$. Zeitschrift fuer Naturforschung, Teil B. Anorganische Chemie, Organische Chemie 1996;51:29-31. Crystallography Open Database: www.crystallography.net/2002761.html

[34] Shim J, Lee CR, Lee HK, Lee JS, Caims EJ. Electrochemical charcteristics of Pt-WO_3/C and Pt-TiO_2/C electrocatalysts in a polymer electrolyte fuel cell. J Power Sources 2001;102:172-177.

[35] Cui X, Guo L, Cui F, He Q, Shi J. Electrocatalytic activity and CO-tolerance properties of mesostructured Pt/WO_3 composite as an anode catalyst for PEMFCs. J Phys Chem C 2009;113:4134-4138.

[36] Tseung ACC, Shen PK, Chen KY. Precious metal/hydrogen bronze anode catalysts for the oxidation of small organic molecules and impure hydrogen. J Power Source 1996;61:223-225.

[37] Nagy G, Schiller R. Hydrogen in tungsten bronzes: mechanism of hydrogen intercalation. Int J Hydrogen Energy 1989;14:567-572.

[38] Zeng J, Lee JY. Ruthenium-free, carbon-supported cobalt and tungsten containing binary & ternary Pt catalysts for the anodes of direct methanol fuel cells. Int J Hydrogen Energy 2007; 32:4389-4396.

[39] Santiago EI, Camara GA, Ticianelli EA. CO tolerance on PtMo/C electrocatalysts prepared by the formic acid method. Electrochim Acta 2003;48:3527-3534.

[40] Mukerjee S, Urian RC. Bifunctionality in Pt alloy nanocluster electrocatalysts for enhanced methanol oxidation and CO tolerance in PEM fuel cells: electrochemical and in situ synchrotron spectroscopy. Electrochim Acta 2002;47: 3219-3231.

[41] Justin P, Rao GR. Methanol oxidation on MoO_3 promoted Pt/C electrocatalyst. Int J Hydrogen Energy 2011;36:5875-5884.

[42] Zhou ZH, Li WS, Fu Z, Xiang XD. Carbon nanotube-supported Pt-H_xMoO_3 as electrocatalyst for methanol oxidation. Int J Hydrogen Energy 2010;35:936-941.

[43] Elezović NR, Gajić-Krstajić LjM, Vračar LjM, Krstajić NV. Effect of chemisorbed CO on MoO_x-Pt/C electrode on the kinetics of hydrogen oxidation reaction. Int J Hydrogen Energy 2010;35:12878-12887.

[44] Maillard F, Peyrelade E, Soldo-Olivier Y, Chatenet M, Chaînet E, Faure R. Is carbon-supported Pt-WO_x composite a CO-tolerant material? Electrochim Acta 2007;52:1958-1967.
[45] Ordóñez LC, Roquero P, Sebastian PJ, Ramírez J. CO oxidation on carbon-supported PtMo electrocatalysts: Effect of the platinum particle size. Int J Hydrogen Energy 2007;32:3147-3153.
[46] Alcaide F, Álvarez G, Tsiouvaras N, Peña MA, Fierro JLG, Martínez-Huerta MV. Electrooxidation of H_2/CO on carbon-supported PtRu-MoO_x nanoparticles for polymer electrolyte fuel cells. Int J Hydrogen Energy 2011;36:14590-14598.
[47] Jayaraman S, Jaramillo TF, Baeck SH, McFarland EW. Synthesis and characterization of Pt-WO_3 as methanol oxidation catalysts for fuel cells. J Phys Chem B 2005;109:22958-22966.
[48] Esfahani RAM, Vankova SK, Monteverde Videla AHA, Specchia S. Innovative carbon-free low content Pt catalyst supported on Mo-doped titanium suboxide (Ti_3O_5-Mo) for stable and durable oxygen reduction reaction. Appl Catal B: Environ 2017; 201:419-429.
[49] Baltrusaitis J, Mendoza-Sanchez B, Fernandez V, Veenstra R, Dukstiene N, Roberts A, Fairley N. Generalized molybdenum oxide surface chemical state XPS determination via informed amorphous sample model. Appl Surf Sci 2015;326:151-161.
[50] Schroeder T, Zegenhagen J, Magg N, Immaraporn B, Freund HJ. Formation of a faceted MoO_2 epilayer on Mo(112) studied by XPS, UPS and STM. Surf Sci 2004; 552:85-97.
[51] Scanlon DO, Watson GW, Payne DJ, Atkinson GR, Egdell RG, Law DSL. Theoretical and Experimental Study of the Electronic Structures of MoO_3 and MoO_2. J Phys Chem C 2010;114:4636-4645.
[52] Samjeske G, Wang H, Löffler T, Baltruschat H. CO and methanol oxidation at Pt-electrodes modified by Mo. Electrochim Acta 2002;47:3681-3692.
[53] Guillén-Villafuerte O, García G, Rodríguez JL, Pastor E, Guil-López R, Nieto E, Fierro JLG. Preliminary studies of the electrochemical performance of Pt/X@MoO_3/C (X= Mo_2C, MoO_2, Mo^0) catalysts for the anode of a DMFC: Influence of the Pt loading and Mo-phase. Int J Hydrogen Energy 2013;38:7811-7821.
[54] Tsiouvaras N, Martínez-Huerta MV, Paschos O, Stimming U, Fierro JLG, Peña MA. PtRuMo/C catalysts for direct methanol fuel cells: Effect of the pretreatment on the structural characteristics and methanol electrooxidation. Int J Hydrogen Energy 2010;35:11478-11488.
[55] Pantea D, Darmstadt H, Kaliaguine S, Roy C. Electrical conductivity of conductive carbon blacks: influence of surface chemistry and topology. Appl. Surf. Sci. 2003;217:181-193.

[56] Barroso-Bogeat A, Alexandre-Franco M, Fernndez-Gonzalez C, Macias-Garcia A, Gomez-Serrano V. Electrical conductivity of activated carbon-metal oxide nanocomposites under compression: a comparison study. Phys Chem Chem Phys 2014;16:25161-25175.

[57] Park KW, Seol KS. Nb-TiO_2 supported Pt cathode catalyst for polymer electrolyte membrane fuel cells. Electrochem Commun 2007;9:2256-2260.

[58] Hu JE, Liu Z, Eichhorn BW, Jackson GS. CO tolerance of nano-architectured Pt-Mo anode electrocatalysts for PEM fuel cells. Int J Hydrogen Energy 2012;37:11268-11275.

[59] Pereira LGS, Paganin VA, Ticianelli EA. Investigation of the CO tolerance mechanism at several Pt-based bimetallic anode electrocatalysts in a PEM fuel cell. Electrochim Acta 2009;54:1992-1998.

Supplementary material for

Preparation of CO-tolerant anode electrocatalysts for polymer electrolyte membrane fuel cells

D. Gubán[1], A. Tompos[1], I. Bakos[1], Á. Vass[1], Z. Pászti[1], E.Gy. Szabó[1], I.E. Sajó[2], I. Borbáth[1*]

[1]*Institute of Materials and Environmental Chemistry, Research Centre for Natural Sciences, Hungarian Academy of Sciences, H-1117 Budapest, Magyar tudósok körútja 2, Hungary*
[2]*University of Pécs, Szentágothai Research Centre, Pécs, H-7624, Ifjúság str. 20. Hungary*

1. Details of experimental methods and procedures

1.1. Short description of the preparation of $Ti_{(1-x)}M_xO_2$-C (M=W, Mo) composites

Some details of the preparation of the $Ti_{(1-x)}M_xO_2$-C (M=W, Mo) composites is given here; for a more detailed description see Refs. [1,2].

During the synthesis of the composite first transparent acidic TiO_2 colloidal solution was made by adding concentrated HNO_3 to a vigorously stirred mixture of titanium-isopropoxide and distilled water. In route ***A*** (see Fig. 1 of the main text) active carbon (CABOT, Black Pearls 2000) was added after 4 h stirring at room temperature (RT). In order to facilitate the formation of rutile nuclei, the mixture was aged at RT for 4 days. After the aging, $(NH_4)_6H_2W_{12}O_{40}$ was added and the solution was evaporated at 80°C. As shown in Fig. 1 of the main text in route ***B*** the order of active carbon and W precursor compound addition was changed: first $(NH_4)_6H_2W_{12}O_{40}$ was added to TiO_2 colloidal solution and then, after 4 days of aging, active carbon was introduced. In both cases the powder was dried at 80°C overnight. Preparation of the $Ti_{0.7}Mo_{0.3}O_2$-C composites was done using route ***A*** (see Fig. 1 of the main text).

1.2. Details of the Pt loading

Pt loading was achieved using modified $NaBH_4$-assisted ethylene-glycol (EG) reduction method using $Ti_{(1-x)}M_xO_2$-C (M=W, Mo) composites as support and ethanol as a solvent [1,2]. It should be noted that in Ref. [3] ethylene glycol (EG) was used as a solvent for Pt precursor. The platinum content was 40 wt%.

H_2PtCl_6 (333 mg) was solved in 50 ml ethanol and 200 mg of the support material was suspended in the solution. A solution prepared by the reaction of $NaBH_4$ (590 mg) and EG (7.4 ml) was added dropwise to the suspension at 65 °C with stirring. After 3 hours of stirring at 65°C, 30 ml 0.5 M HCl was added to the suspension and stirred for an additional 2.5 hours at RT to deposit the Pt particles onto the support material. The material was washed with water by centrifugation and dried at 80 °C overnight.

1.3. Methods of physical characterization

The powder X-ray diffraction (XRD) patterns were obtained in a Philips model PW 3710 based PW 1050 Bragg-Brentano parafocusing goniometer using CuK_α radiation (λ= 0.15418 nm), graphite monochromator and proportional counter. Silicon powder (NIST SRM 640) was used as an internal standard and the scans were evaluated with profile fitting methods. The cell parameters of the crystalline phases were determined from the fitted d-

* Corresponding author, Tel.: +36 1 382 6916, email: borbath.irina@ttk.mta.hu, address: H-1519 Budapest, P.O.Box 286, Hungary (Irina Borbáth)

values. Crystallite sizes were calculated from reflection line broadening using the Scherrer-equation.

Transmission Electron Microscopy (TEM) studies of the samples were made by use of a FEI Morgagni 268D type transmission electron microscope (accelerating voltage: 100 kV, W-filament). The fresh samples were prepared by grinding and dispersing of the resulted powder in ethanol. After electrochemical experiments catalysts were removed from the electrodes with isopropanol. A volume of the obtained suspension was pipetted onto a carbon coated copper grid. The average diameter was calculated by measuring the diameters of no less than 700 randomly selected metal particles from the non-aggregated areas in at least tree micrographs of each sample.

Temperature Programmed Reduction (TPR) experiments were carried out in a commercial equipment (ASDI RXM 100- Advanced Scientific Designs Inc.) with a quartz flow reactor. A thermal conductivity detector was adapted to monitor the H_2 consumption during a TPR run. The profiles were automatically recorded with a computer and the area under the TPR curve was integrated. The quantity of the H_2 consumption was evaluated by calibrating the detector with a well-known volume and concentration of hydrogen containing gas mixture. The samples were heated at 10ºC min^{-1} from room temperature up to 750ºC. The reductive mixture (5.2 v/v % H_2-Ar) was introduced to the reactor with a flow rate of 40 cm^3 min^{-1}.

X-ray photoelectron spectroscopy (XPS) measurements were performed on the $Ti_{0.7}Mo_{0.3}O_2$-C composite. The experiments were carried out using an EA125 electron spectrometer (OMICRON Nanotechnology GmbH, Germany). The photoelectrons were excited by non-monochromatized MgKα (1253.6 eV) radiation. Spectra were recorded in the Constant Analyser Energy mode of the energy analyser with 30 eV pass energy resulting in a spectral resolution of 1 eV. The powder samples were suspended in isopropanol; drops of this suspension were placed on standard OMICRON sample plates. Binding energies were referenced to the main component of the C 1s spectrum of the support (graphite at 284.4 eV binding energy). Data were processed using the CasaXPS software package [4] Nominal surface compositions were calculated using the XPS MultiQuant software package [5,6]. Chemical states were identified by XPS databases [7,8] and with the help of the related literature.

1.4. Electrochemical characterization

Pt-based electrocatalysts supported on $Ti_{(1-x)}M_xO_2$-C composite materials were investigated by means of cyclic voltammetry (CV) and CO_{ad} stripping technique in conventional three-electrode electrochemical glass cell using a Biologic SP150 potentiostat and the EC-LAB software package. The applied electrolyte was 0.5 mol dm^{-3} (M) H_2SO_4. The electrolyte solution was prepared with Milli-Q water (Millipore, 18.2 MΩ cm, total organic compounds <3 ppb) and concentrated H_2SO_4 (Merck, P.A., 96%). Ar gas (99.9995 %) was used for deoxigenation.

The working electrode was prepared dipping a drop (3.6 μl) of catalyst ink on a freshly polished glassy carbon (GC) electrode (d = 0.3 cm, geometric surface area A = 0.0707 cm^2), and air-dry at RT for 30 minutes. Before each test the GC disc was polished with 0.05 μm gamma alumina to obtain a mirror finish, followed by ultrasonic cleaning in water, isopropanol and again water to remove any traces of organic impurities.

For the catalyst ink 5 mg catalyst sample was suspended in 4 ml H_2O (18.2 MΩ cm) + 1 ml isopropanol (Molar Chemicals, 99.5%) + 20 μl Nafion solution (D520 Nafion Dispersion - Alcohol based 1000 EW at 5 wt%, DuPont™ Nafion®). Pt loading of the electrodes was 20 μg cm^{-2}. The reference electrode was a hydrogen electrode immersed in the same electrolyte

as the working electrode and all potentials are given on the RHE scale. Pt wire was used as a counter electrode.

In order to get information on the initial behavior of the electrocatalysts, CO_{ads} stripping voltammetry measurements were carried out on the samples without any electrochemical pre-conditioning or cleaning, and after the so-called "pre-leaching" treatment.

Gaseous CO was fed into the cell for 30 min while maintaining a constant potential of 50 mV. After CO removal (argon purge for 30 min), the working electrode was subjected to a cyclic voltammetry step at a 10 mV s^{-1} scan rate between 50 and 1000 mV. After the first CO stripping measurements the electrode was subjected to the "pre-leaching" procedure, by means of performing cyclic polarization with 50 mV s^{-1} for 35 cycles in the potential window between 50 and 1000 mV. Then the above described CO stripping measurement was repeated. After the second CO_{ads} stripping measurement the cyclic voltammogram was recorded again. Relative errors were calculated as the standard deviation of at least three independent measurements.

Catalytic activity of the catalyst samples was tested in the HOR by rotating disk electrode (RDE) technique at 225 rpm in hydrogen saturated 0.5 M H_2SO_4 solution at ambient temperature and pressure using a PAR 283 potentiostat. Pure and 100 ppm CO containing H_2 were used. GC electrode of 5 mm diameter (geometric surface area: 0.196 cm^2) was used in these measurements. 10 μl catalyst ink was dropped on the freshly polished GC electrode which resulted in about 20 μg cm^{-2} Pt loading. The reference electrode was a hydrogen electrode. Pt sheet was used as a counter electrode.

1.5. Electrochemical single cell measurements

Fuel cell polarization measurements were carried out at 85±4ºC using Bio-Logic and Paxitech FCT-150S test device. For PEMFC single cell tests, membrane electrode assemblies (MEAs) with catalyst coated gas diffusion layer and geometric area of 16 cm^2 were prepared by screen printing method. Teflon loaded carbon paper (H23C6, Freudenberg FCCT) was used for gas diffusion electrodes preparation.

In all measurements commercial 40 wt% Pt/C (Q) catalyst was used as cathode. The weight ratio of the Nafion resin to the catalysts (dry weight) was 1/1.85 and correspondingly the ionomer/carbon weight ratio was ca. 0.8-0.9/1. The loading of metal catalysts in both electrodes was 0.4 mg_{Pt} cm^{-2}. All catalyst loadings are referenced to the geometric surface area of the membrane. The catalysts were suspended and ultrasonically mixed in EG, isopropanol and 5 % Nafion solution to form homogeneous ink. Usually the catalyst loading procedure was repeated two or three times, followed by drying in vacuum at 110^{o}C for 12 hours.

MEAs were assembled by hot pressing the anode and cathode catalyst coated electrodes onto each side of a proton-conducting Nafion membrane (Nafion XL, Ion Power) using manual hydraulic press (Specac Inc., P/N GS15011) with heated platens (Specac Inc., P/N GS15515) at 120^{o}C under 57.3 kg cm^{-2} for 3 minutes.

Prior polarization measurements the MEA was activated at 0.6 V until the current stabilized (4-5 hours) with cell temperature 85^{o}C. The flow of gases was 120 ml min^{-1}; the gas pressure was 2 bar. The polarization measurements were performed with the cell at 85^{o}C, the relative humidity for oxygen and hydrogen was 82 %. To obtain a polarization curve the potential was measured as the function of current. At first the current was set to 0 A for 10 s, then it was increased with 12.5 mA cm^{-2} increment for 10-10 s and the potential response was measured. The poisoning resistance of our catalyst was studied using 100 ppm CO/H_2 mixture. The activities of the samples were compared with those observed on commercial 40 wt% Pt/C (Q) and PtRu/C (Q) references.

2.1. Characterization of the Pt/$Ti_{(1-x)}W_xO_2$-C electrocatalysts

As shown in Fig. S1 upon decrease of the potential limit from 1250 mV to 1000 mV during polarization of the Pt/3-W-B catalyst for 35 cycles the intensity of the anodic peak connected to the oxidation of tungsten bronze remains practically unchanged, thereby demonstrating relative stability of this catalyst up to 1000 mV.

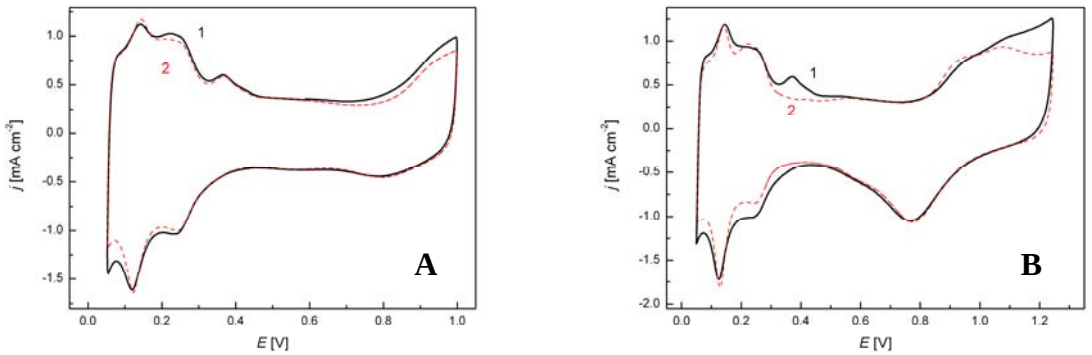

Fig. S1. Cyclic voltammograms of the Pt/3-W-B electrode in 0.5 M H_2SO_4. (A) 1: 1st CV of a freshly prepared electrode, 2: CV after 35 cycles between 50-1000 mV potential limits. (B) 1st CV (1) and the 35th (2) CV polarizing the electrode between 50-1250 mV potential limits. Sweep rate: 50 mV s^{-1}.

References

[1] Gubán D, Borbáth I, Pászti Z, Sajó IE, Drotár E, Hegedűs M, Tompos A. Preparation and characterization of novel $Ti_{0.7}W_{0.3}O_2$-C composite materials for Pt-based anode electrocatalysts with enhanced CO tolerance. Appl Catal B-Environ 2015;174:455-470.

[2] Gubán D, Pászti Z, Borbáth I, Bakos I, Drotár E, Sajó IE, Tompos A. Design and preparation of CO tolerant anode electrocatalysts for PEM fuel cells. Period Polytech- Chem 2016;60:29-39.

[3] Kim P, Joo JB, Kim W, Kim J, Song IK, Yi, J. $NaBH_4$-assisted ethylene glycol reduction for preparation of carbon-supported Pt catalyst for methanol electro-oxidation. J Power Sources 2006;160: 987-990.

[4] Fairley N. "CasaXPS: Spectrum Processing Software for XPS, AES and SIMS," Version 2.3.13, Casa Software Ltd, Cheshire. 2006. http://www.casaxps.com

[5] Mohai M. "XPS MultiQuant: Multimodel XPS Quantification Software," Surface and Interface Analysis 36(8), pp. 828-832. 2004.

[6] Mohai M. "XPS MultiQuant: Multi-model X-ray photoelectron spectroscopy quantification program," Version 3.00.16. 2003.

[7] Wagner CD, Naumkin AV, Kraut-Vass A, Allison JW, Powell CJ, Rumble JR. Jr. „NIST X-ray Photoelectron Spectroscopy Database," Version 3.4, National Institute of Standards and Technology, Gaithersburg, MD, 2003.

[8] Moulder JF, Stickle WF, Sobol PE, Bomben K.D. "Handbook of X-ray Photoelectron Spectroscopy," Perkin-Elmer Corp., Eden Prairie, Minnesota, USA. 1992.